مجلة جامعة تشرين للدراسات والبحوث العلمية
المجلد الرابع ـ العدد الثاني من ٦١ الى ٨٤

شوال ١٤٠١
آب ١٩٨١

السلوك اللدن للمنشآت المعدنية المعرضة في آن واحد إلى ضغط وفتل.

الدكتور وسيم بورعي
كلية الهندسة

تتمة ما نشر في العدد الاول .

ان استخدام الفولاذ في المنشآت المعدنية والصناعية والبحرية المعرضة في آن واحد الى جهود ضغط وفتل يستلزم معرفة سلوك المادة الفولاذية المستخدمة في التصميم في منطقتي اللدونة المضطربة (PLASTIC RANGE) ومنطقة التماسك ذات التشوهات الكبيرة مما يستوجب صياغة دقيقة للحالات الحدية المؤدية الى انهيار العنصر الانشائي .

وان معرفة خواص الفولاذ الميكانيكية في المنطقتين سابقتي الذكر هو امر اساسي لتصميم القطع الانشائية وحسابها على الاستقرار بالاضافة الى تحقيق وفر اقتصادي كبير في التصميم .

يعالج البحث بصورة رئيسية السلوك الفعلي للفولاذ الانشائي صنف (ـ 44 ـ 42) المستعمل بشكل كبير (u_l = 450 ـ 550 Mpa) واساسي في المنشآت المعدنية المعرضة في آن واحد الى جهود ضغط فتل وهذا يتضمن حساب وقياس القيمة الفعلية لعامل القص المماسي $G_t : \frac{d\tau}{d\gamma}$ لمناحي تحميل مختلفة في منطقة الخضوع وايضا في منطقة التماسك ذات التشوهات الكبيرة .

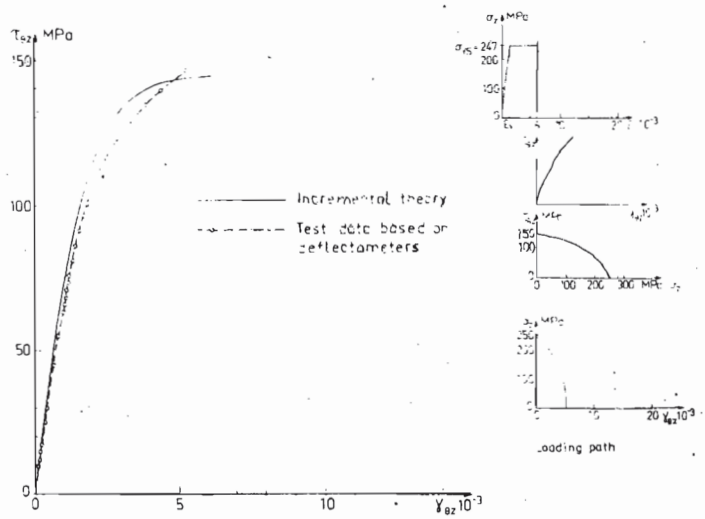

Fig 13 Shear stress $\tau_{\theta z}$ versus shear strain $\gamma_{\theta z}$ for constant axial compressive strain $\varepsilon_z = 6 \cdot 10^{-3}$ within *Lüder's* field, test CT_5. Structural carbon steel SIS 1312

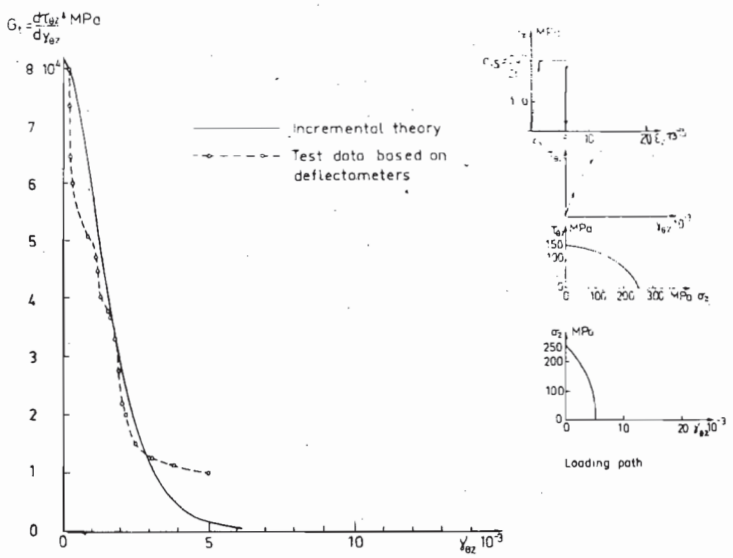

Fig 14 The tangent modulus in shear G_t versus shear strain $\gamma_{\theta z}$ for a constant axial compressive strain within *Lüder's* field, test CT_5. Structural carbon steel SIS 1312

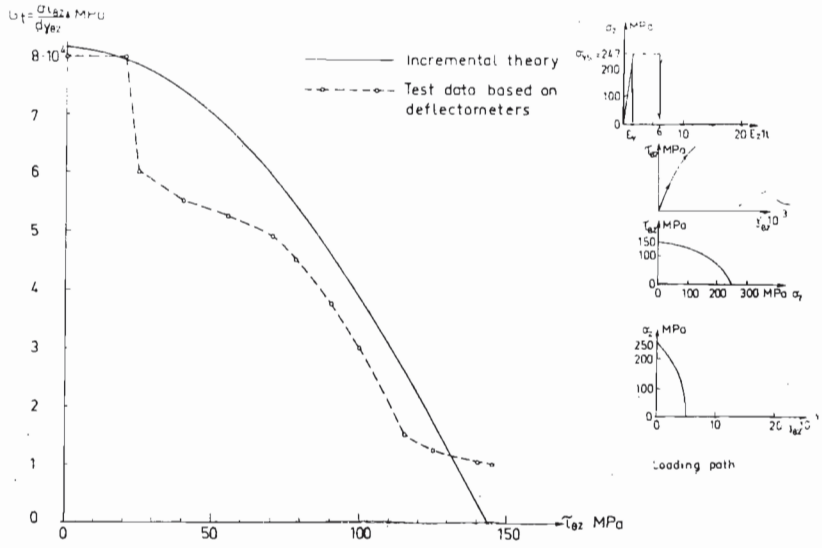

Fig 5 The tangent modulus in shear G_t versus shear stress $\tau_{\theta z}$ for a constant axial compressive strain $\varepsilon_z = 6 \cdot 10^{-3}$ within *Lüder's* field, test CT_5. Structural carbon steel SIS 1312

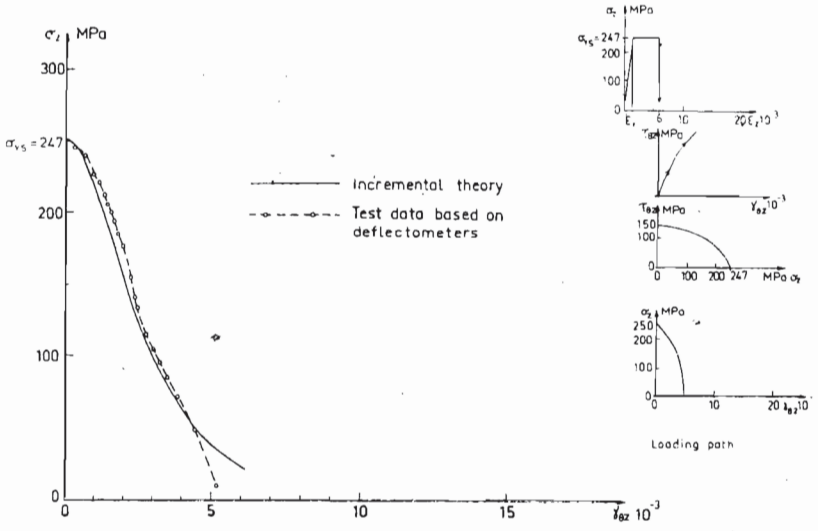

Fig 16 Axial compressive stress σ_z versus shear strain $\gamma_{\theta z}$ for const strain within *Lüder's* field, test CT_5. Structural carbon stee SIS 1312

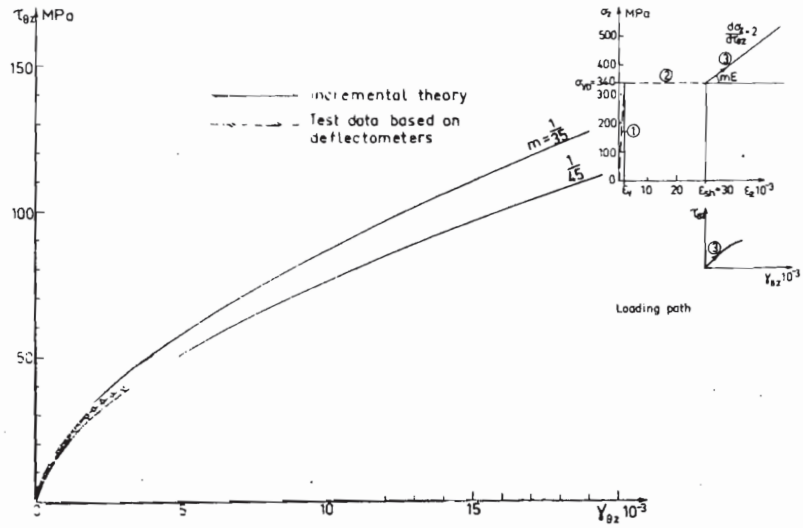

Fig 17 Shear stress $\tau_{\theta z}$ versus shear strain $\gamma_{\theta z}$ for a constant value $\frac{d\sigma}{d\tau} = 2$ in the strain hardening range, test CT_6. Structural carbon steel SIS 1312

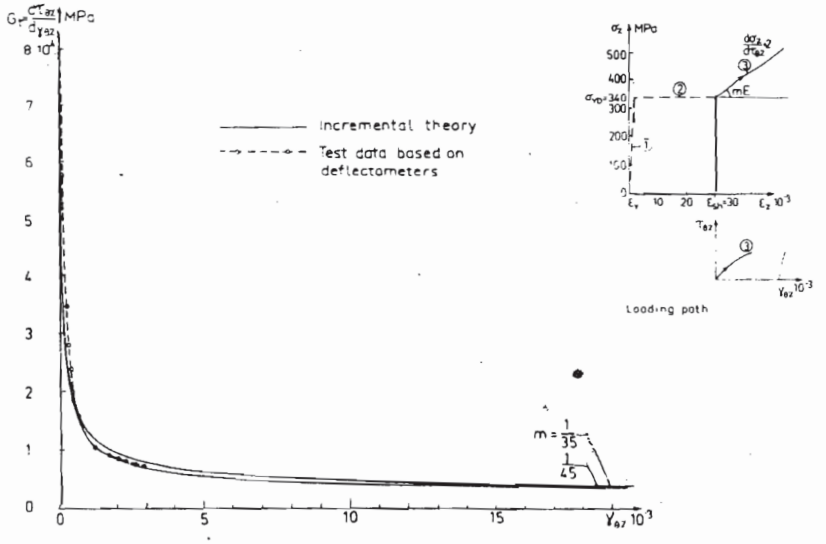

Fig 18 The tangent modulus in shear G_t versus shear-strain $\gamma_{\theta z}$ for constant ratio of $\frac{d\sigma}{d\tau} = 2$ in the strain hardening range, test CT_6. Structural carbon steel SIS 1312

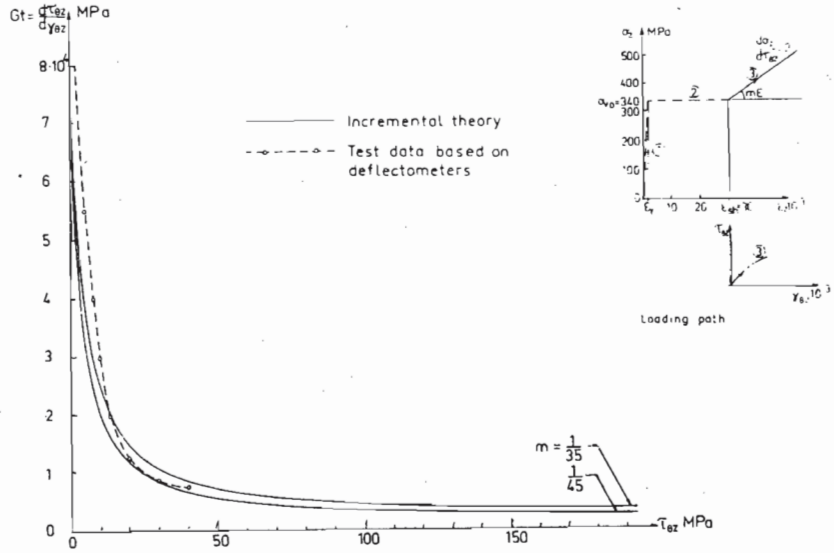

Fig 19 The tangent modulus in shear G_t versus shear stress $\tau_{\theta z}$ for a constant ratio of $\frac{d\sigma}{d\tau} = 2$ in the strain hardening range, test CT_6. Structural carbon steel SIS 1312

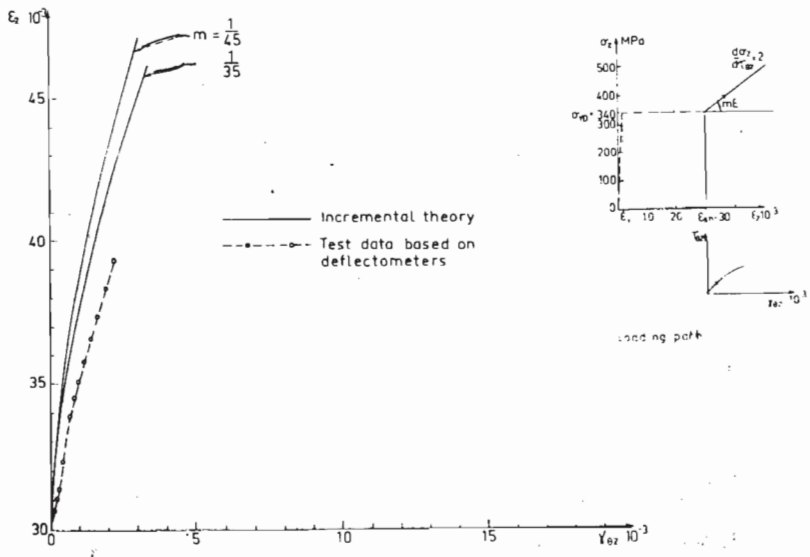

Fig 20 The axial strain ε_z versus shear strain $\gamma_{\theta z}$ for constant ratio $\frac{d\sigma}{d\tau} = 2$ in the strain hardening range, test CT_6. Structural carbon steel SIS 1312

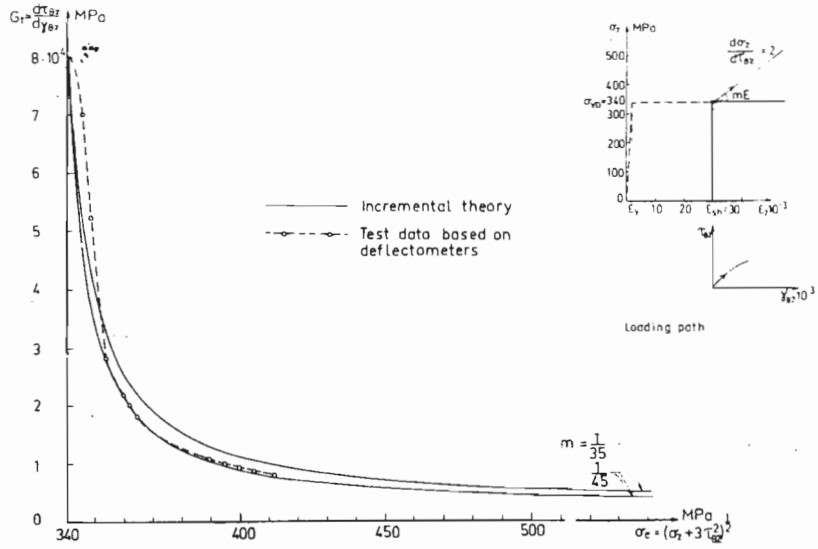

Fig 21 The tangent modulus in shear G_t versus effective stress σ_e for a constant ratio of $\frac{d\sigma}{d\tau} = 2$ in the strain hardening range, test CT_6. Structural carbon steel 1312

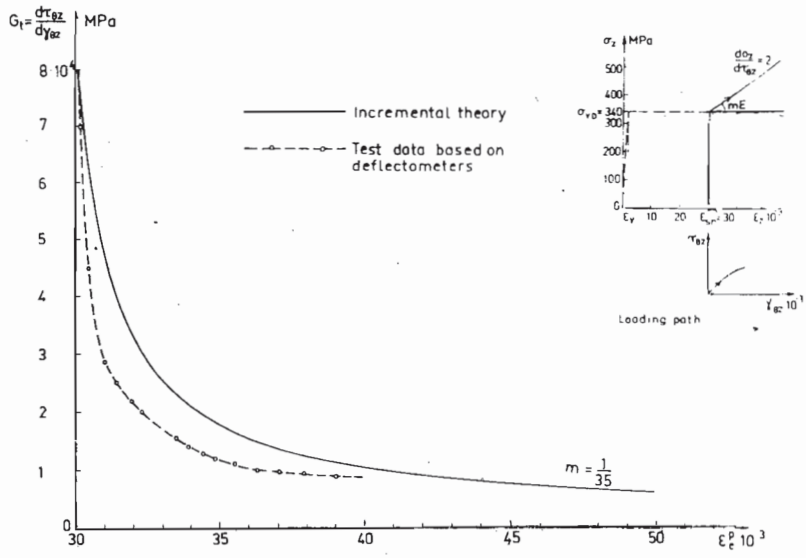

Fig 22 The tangent modulus in shear G_t versus the integrated effective plastic strain increment ε_e^p calculated according to *von Mises* yield criterion and associated flow rule, for a constant ratio $\frac{d\sigma}{d\tau} = 2$ in the strain hardening range, test CT_6. Structural carbon steel SIS 1312

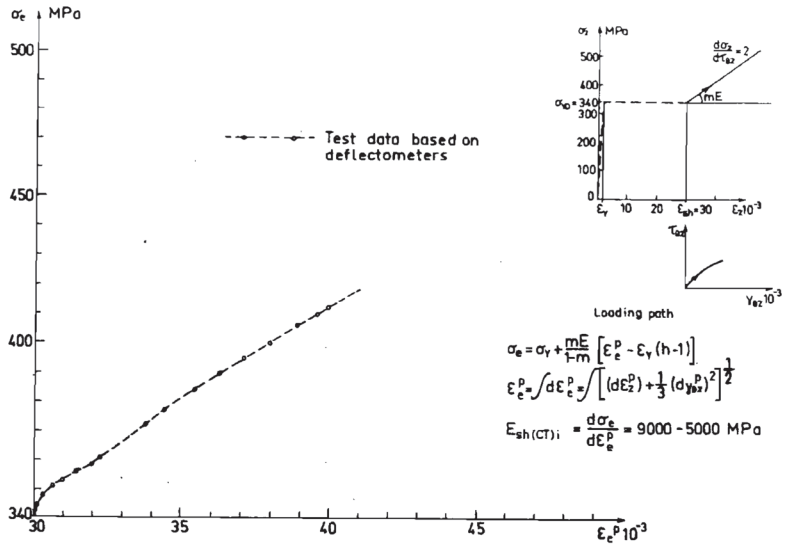

23

Fig Effective stress σ_e versus integrated effective plastic strain increment ε_e^p (calculated according to *von Mises* yield criterion and associated flow rule) for a constant ratio of $\frac{d\sigma}{d\tau} = 2$ in the strain hardening range, test CT_6. Structural carbon steel SIS 1312

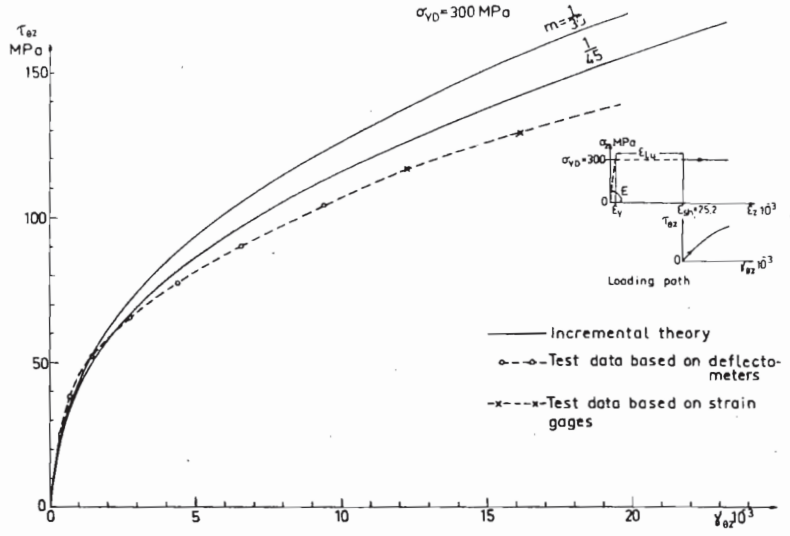

Fig Shear stress $\tau_{\theta z}$ versus shear strain $\gamma_{\theta z}$ for a shear stress $\tau_{\theta z}$ which is superimposed on constant axial compressive yield stress $\sigma_z = -\sigma_Y = -300$ MPa in the strain hardening range, test CT_7. Structural carbon steel SIS 1312

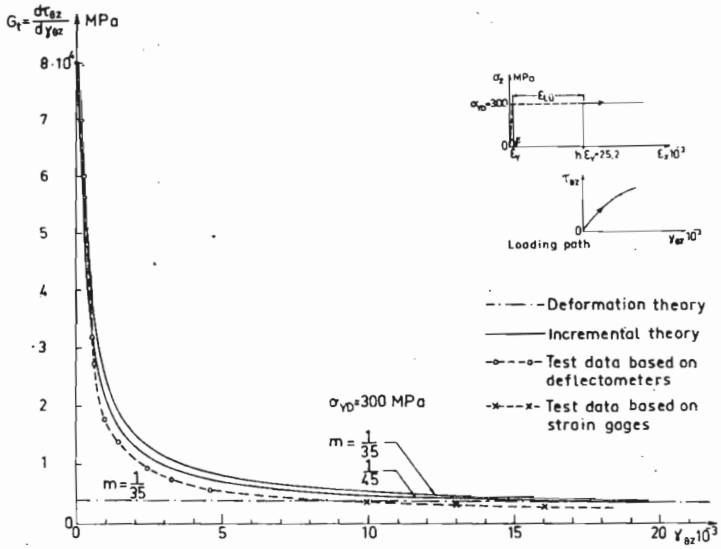

Fig The tangent modulus in shear G_t versus shear strain $\gamma_{\theta z}$ for a shear stress $\tau_{\theta z}$ which is superimposed on a constant axial compressive stress $\sigma_z = -\sigma_Y = -300$ MPa in the strain hardening range, test CT_7. Structural carbon steel SIS 1312

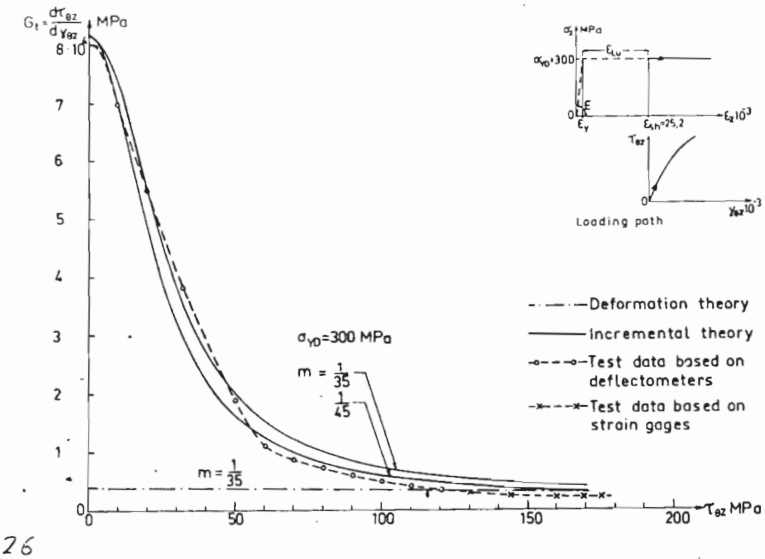

26

Fig The tangent modulus in shear G_t versus shear stress $\tau_{\theta z}$ which is superimposed on a constant axial compressive yield stress $\sigma_z = -\sigma_Y = -300$ MPa in the strain hardening range, test CT_7.
Structural carbon steel SIS 1312

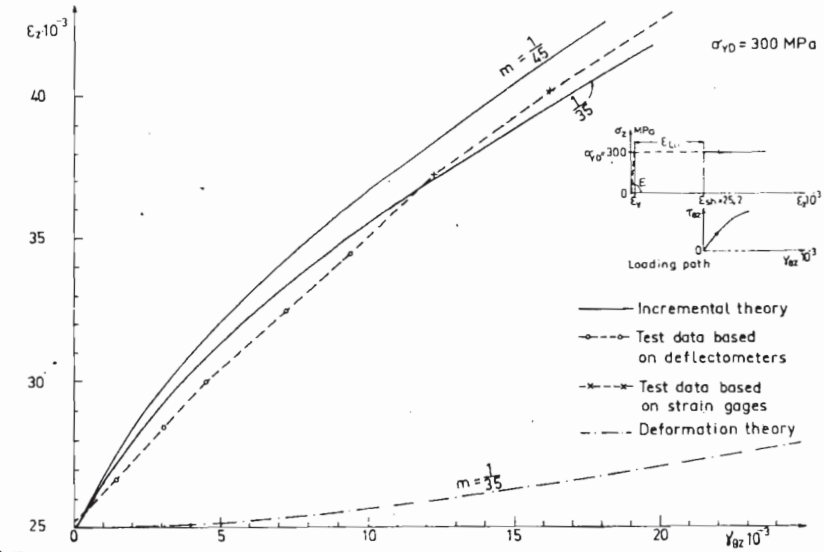

27

Fig The axial strain ε_z versus shear strain $\gamma_{\theta z}$ for a shear stress $\tau_{\theta z}$ which is superimposed on constant axial compressive yield stress $\sigma_z = -\sigma_Y = -300$ MPa in the strain hardening range, test CT_7.
Structural carbon steel SIS 1312

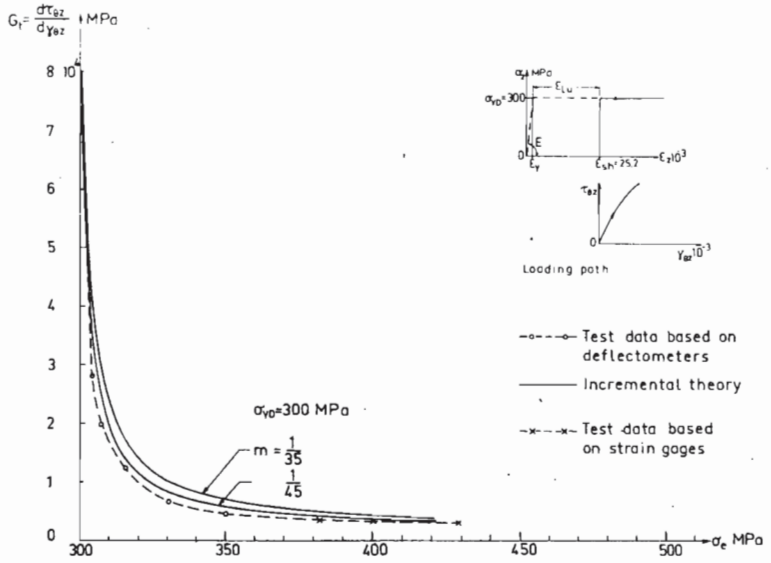

The tangent modulus in shear G_t versus effective stress σ_e for constant shear stress $\tau_{\theta z}$ which is superimposed on a constant axial compressive yield stress $\sigma_z = -\sigma_Y = -300$ MPa in the strain hardening range, test CT_7. Structural carbon steel SIS 1312

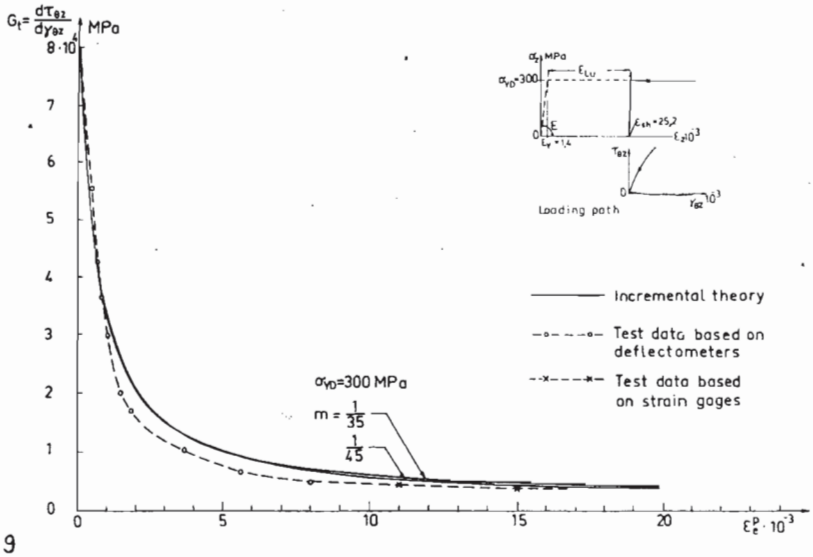

29

The tangent modulus in shear G_t versus the integrated effective plastic strain increment ε_e^p calculated according to *von Mises* yield criterion and associated flow rule, for a shear stress $\tau_{\theta z}$ which is superimposed on constant axial compressive yield stress $\sigma_z = -\sigma_Y = -300$ MPa in the strain hardening range, test CT_7. Structural carbon steel SIS 1312

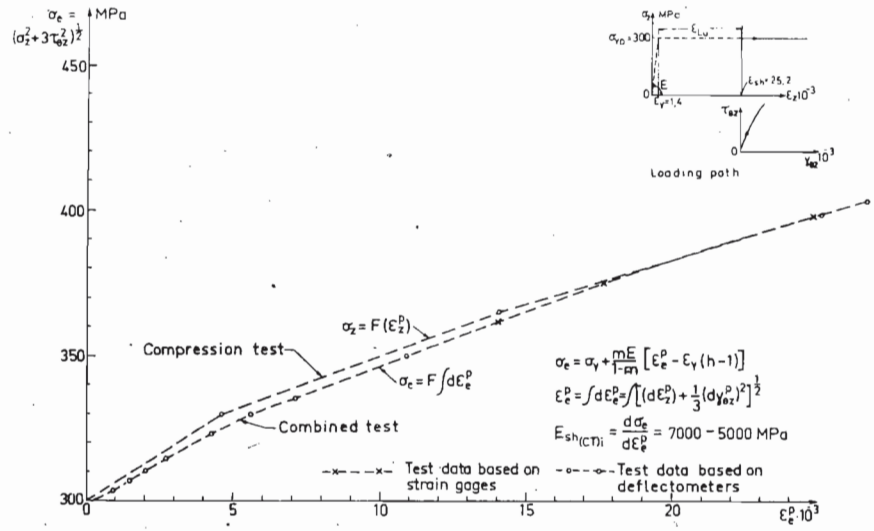

30

Fig Effective stress σ_e versus integrated effective plastic strain increment ε_e^p (calculated according to *von Mises* yield criterion and associated flow rule) for a shear stress $\tau_{\theta z}$ which is superimposed on constant axial compressive yield stress $\sigma_z = -\sigma_y = -300$ MPa in the strain hardening range, test CT_7. Structural carbon steel SIS 1312

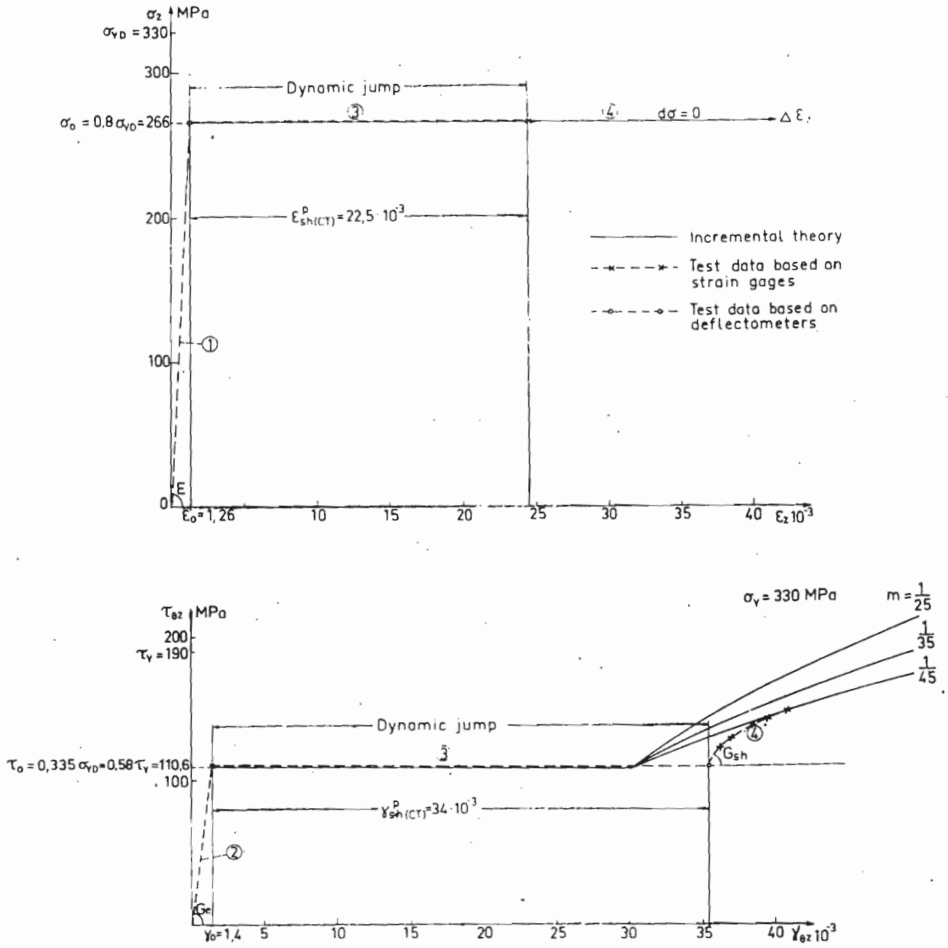

Fig 31 Stress-strain diagrams in the elasto-plastic and strain hardening range for a combination of a constant compressive axial stress σ_0 and a superimposed shear stress τ_0 that gives initial yielding, test CT_8. Structural carbon steel SIS 1312

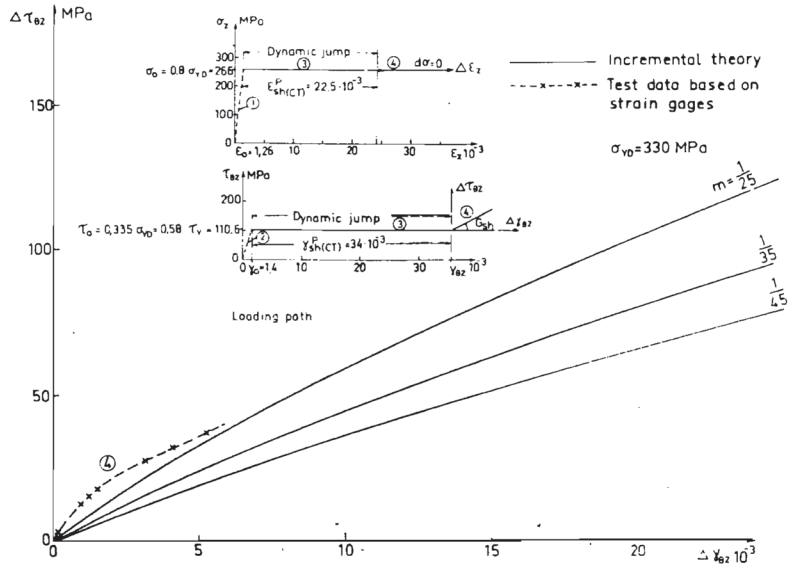

32

Fig Shear stress increment $\Delta\tau_{\theta z}$ versus shear-strain increment $\Delta\gamma_{\theta z}$ in the strain hardening range for a shear stress $\tau_{\theta z}$ which is superimposed on a constant initial axial compressive stress $\sigma_o = 0{,}81\ \sigma_y$, test CT_8. Structural carbon steel SIS 1312

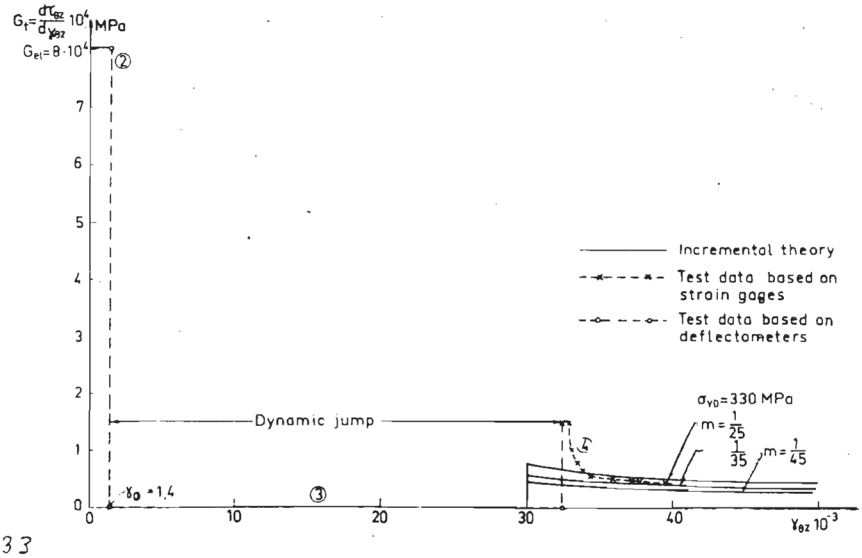

33

Fig The tangent modulus in shear G_t versus shear strain $\gamma_{\theta z}$ in the elasto-plastic and strain hardening range, for a combination of a constant initial compressive axial stress $\sigma_o = 0{,}8\ \sigma_y$ and a superimposed shear stress τ_o that gives initial yielding, test CT_8. Structural carbon steel SIS 1312

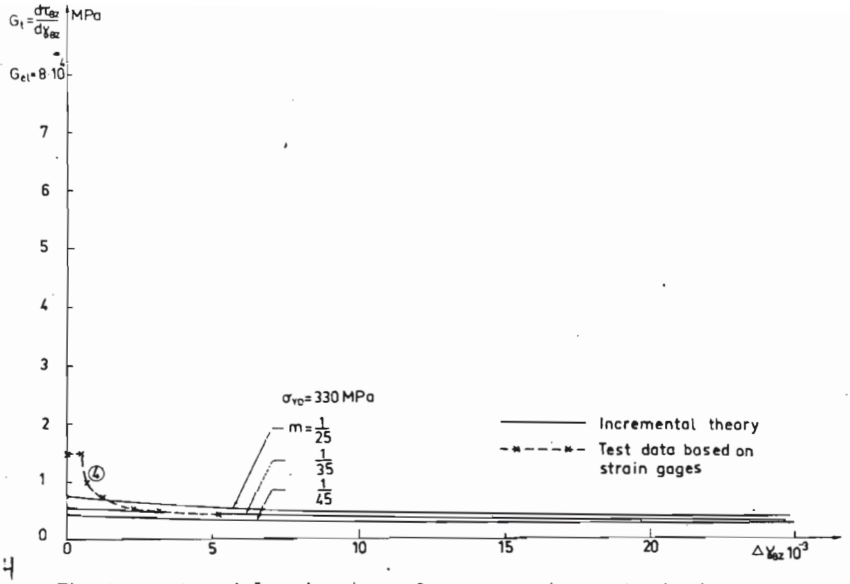

34

Fig The tangent modulus in shear G_t versus shear strain increments $\Delta\gamma_{\theta z}$ in the strain hardening range, for a combination of a constant initial compressive axial stress $\sigma_0 = 0{,}8\ \sigma_Y$ and a superimposed shear stress τ_0 that gives initial yielding, test CT_8. Structural carbon steel SIS 1312

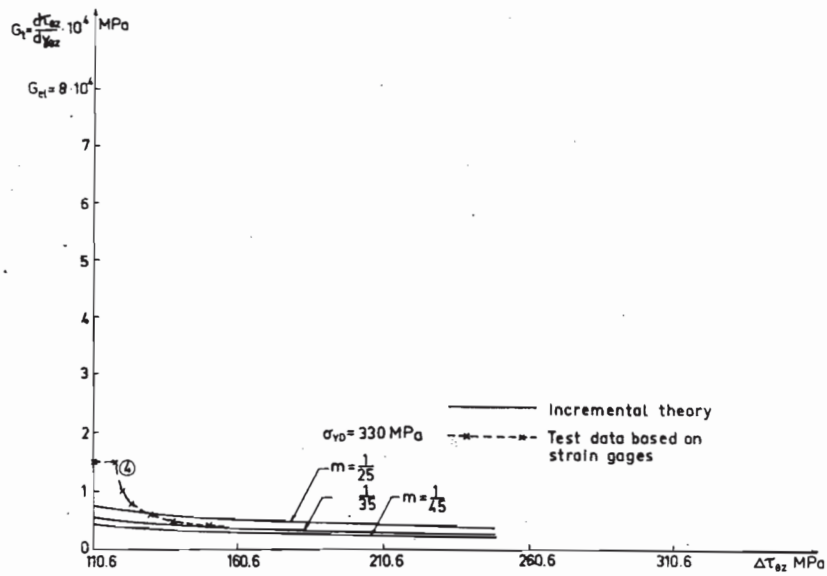

35

Fig The tangent modulus in shear G_t versus shear stress increments $\Delta\tau_{\theta z}$ in the strain hardening range, for a combination of a constant initial compressive axial stress $\sigma_0 = 0{,}8\ \sigma_Y$ and a superimposed shear stress τ_0 that gives initial yielding, test CT_8. Structural carbon steel SIS 1312

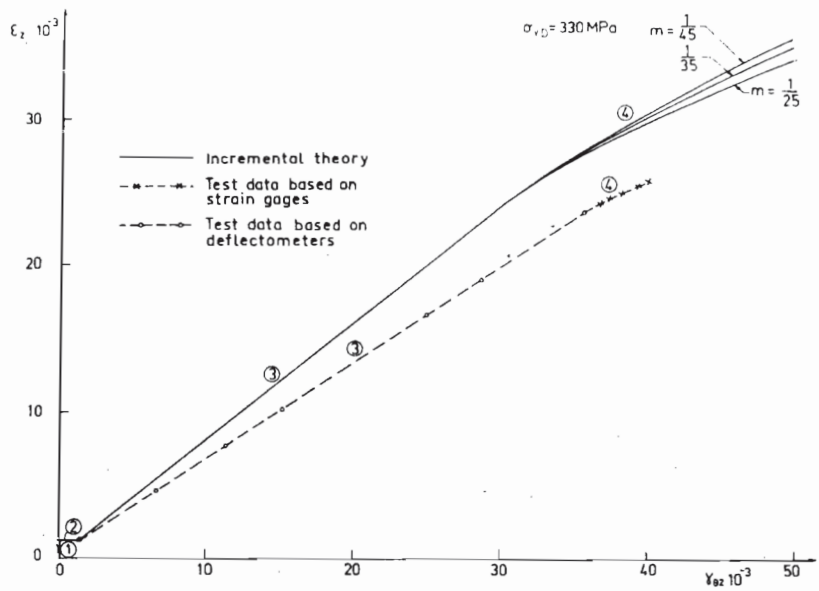

Fig Axial compressive strain ε_z versus shear strain $\gamma_{\theta z}$ in the elasto-plastic and strain hardening range for a combination of a constant initial compressive axial stress $\sigma_o = 0{,}8\ \sigma_Y$ and a superimposed shear stress τ_o that gives initial yielding, test CT_8. Structural carbon steel SIS 1312

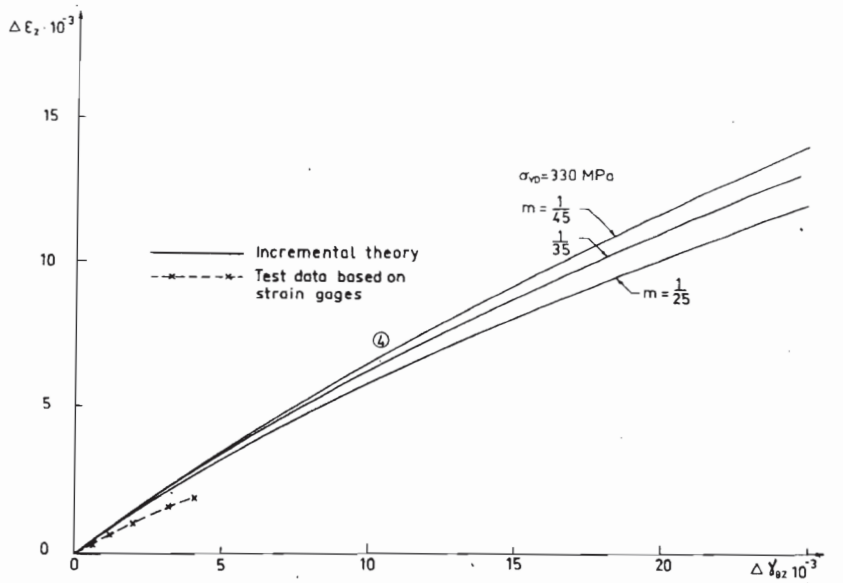

Fig 3.7 Axial compressive strain increments $\Delta\varepsilon_z$ versus shear strain increments $\Delta\gamma_{\theta z}$ in the strain hardening range for a combination of a constant initial compressive axial stress $\sigma_o = 0{,}8\ \sigma_Y$ and a superimposed shear stress τ_o that gives initial yielding, test CT_8. Structural carbon steel SIS 1312

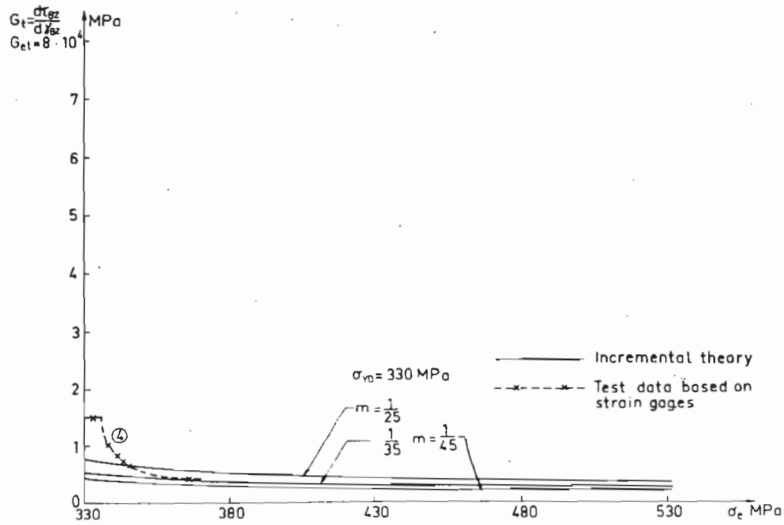

Fig The tangent modulus in shear G_t versus effective stress σ_e in the strain hardening range for a shear stress $\tau_{\theta z}$ which is superimposed on a constant initial compressive axial stress $\sigma_o = 0{,}81\ \sigma_Y$, test CT_8. Structural carbon steel SIS 1312 .

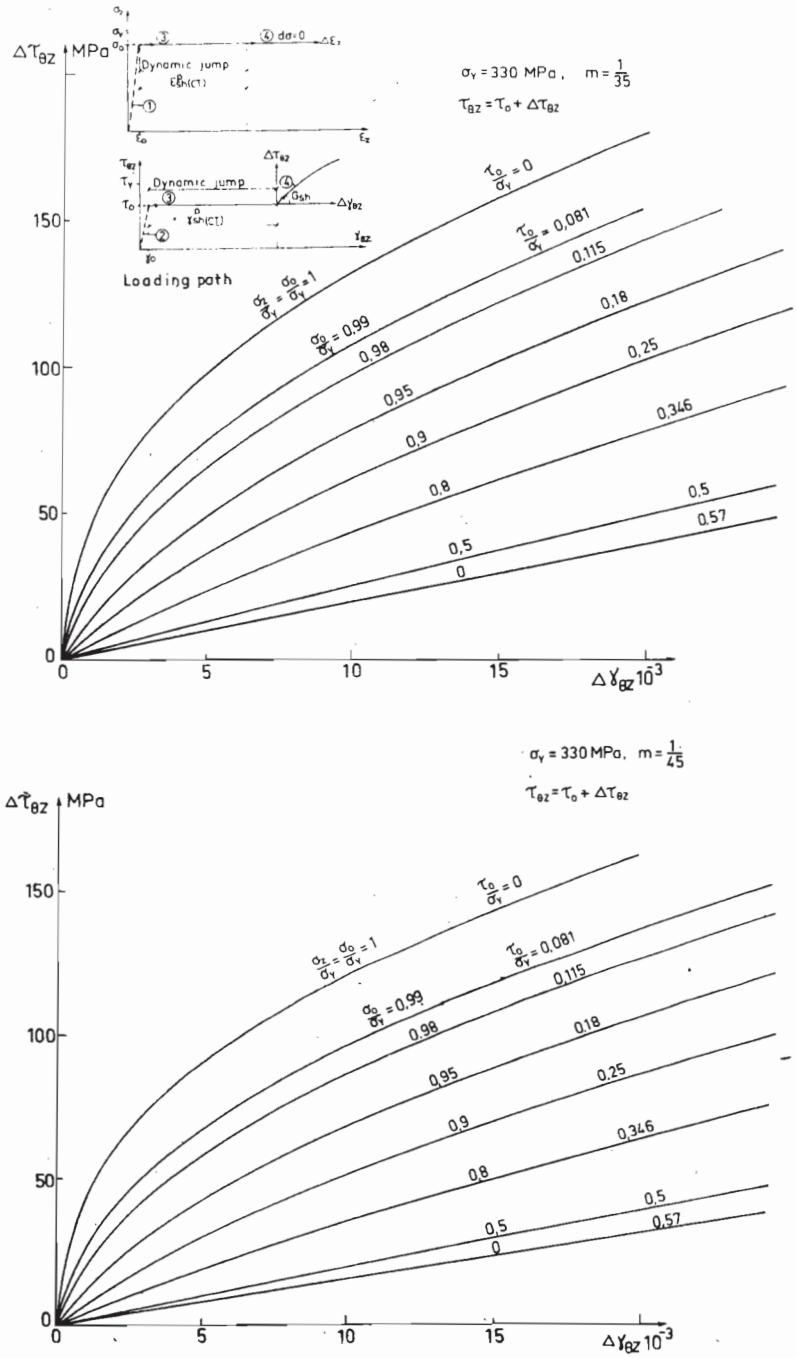

39

Fig Shear stress increments $\Delta\tau_{\theta z}$ versus shear strain increments in the strain hardening range for combinations of a constan compressive axial stress σ_o and a superimposed shear stress that gives initial yielding. Structural carbon steel.

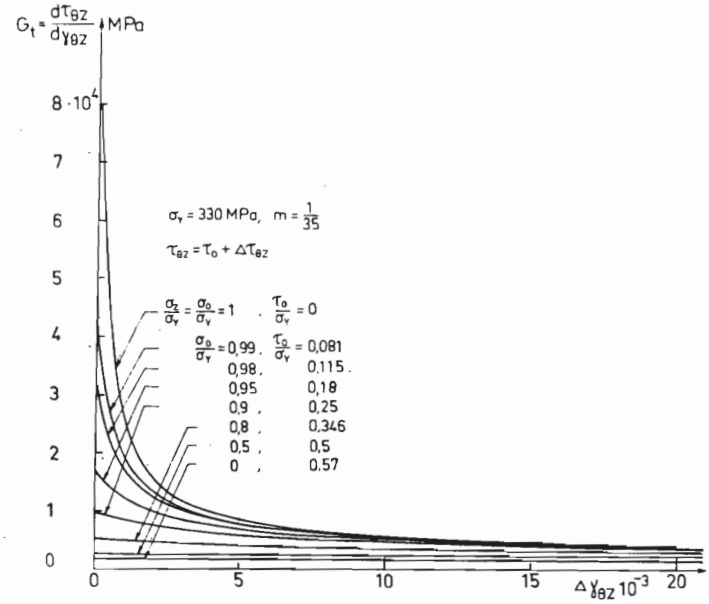

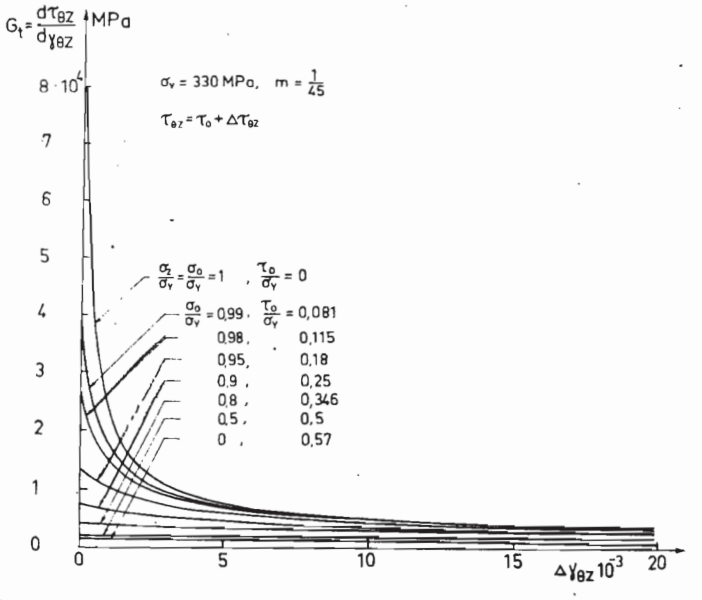

40

Fig The tangent modulus in shear G_t versus shear strain increments $\Delta\gamma_{\theta z}$ in the strain hardening range for combinations of a constant compressive axial stress σ_o and a superimposed shear stress τ_o that gives initial yielding. Structural carbon steel.

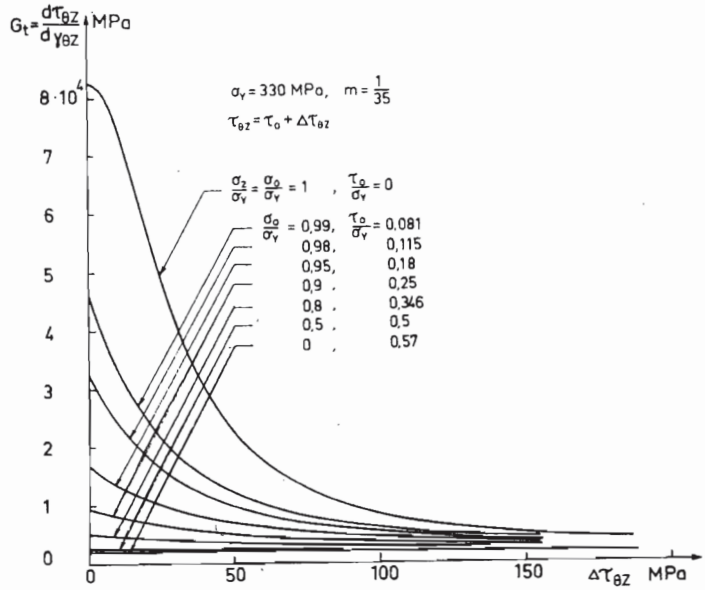

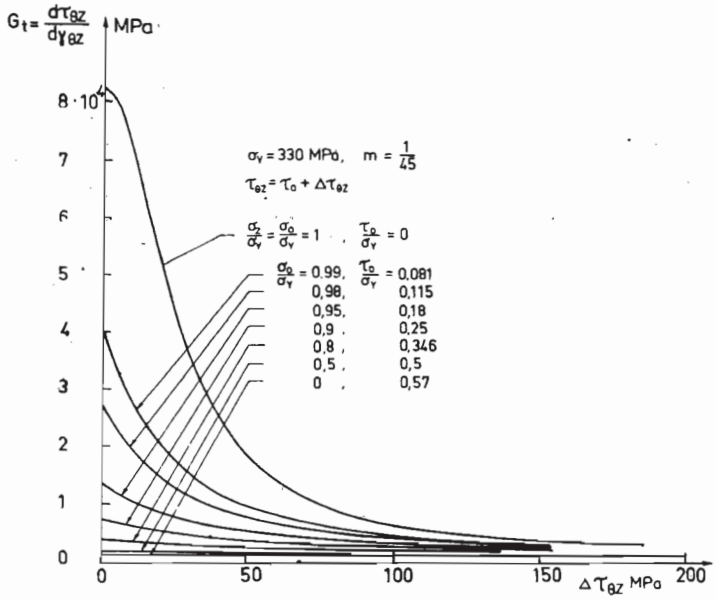

41

Fig The tangent modulus in shear G_t versus shear stress increments $\Delta\tau_{\theta z}$ in the strain hardening range for combinations of a constant compressive axial stress σ_o and a superimposed shear stress τ_o that gives initial yielding. Structural carbon steel.

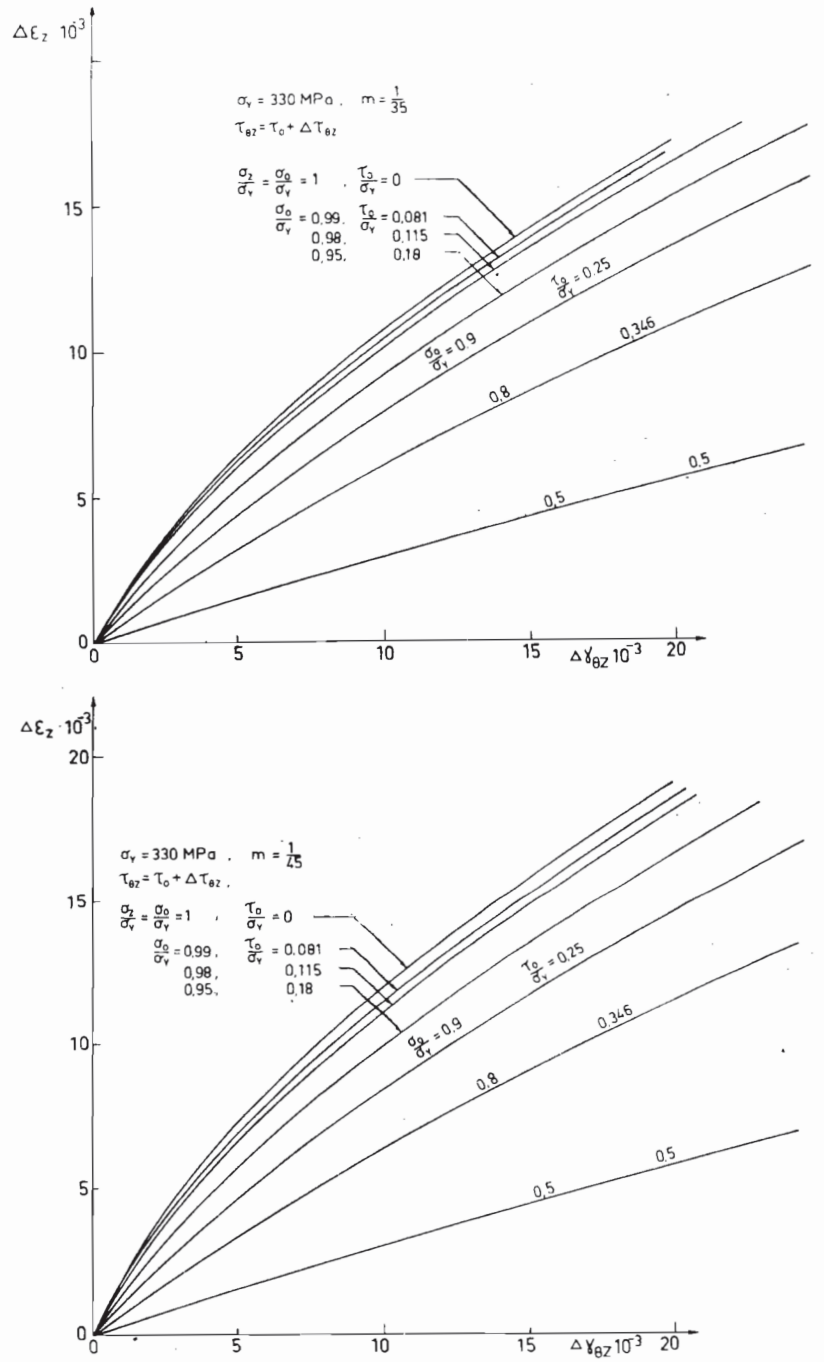

42

Fig. Axial compressive strain increments $\Delta\varepsilon_z$ versus shear strain increments $\Delta\gamma_{\theta z}$ in the strain hardening range for combinations of a constant compressive axial stress σ_o and a superimposed shear stress τ_o that gives initial yielding. Structural carbon steel.

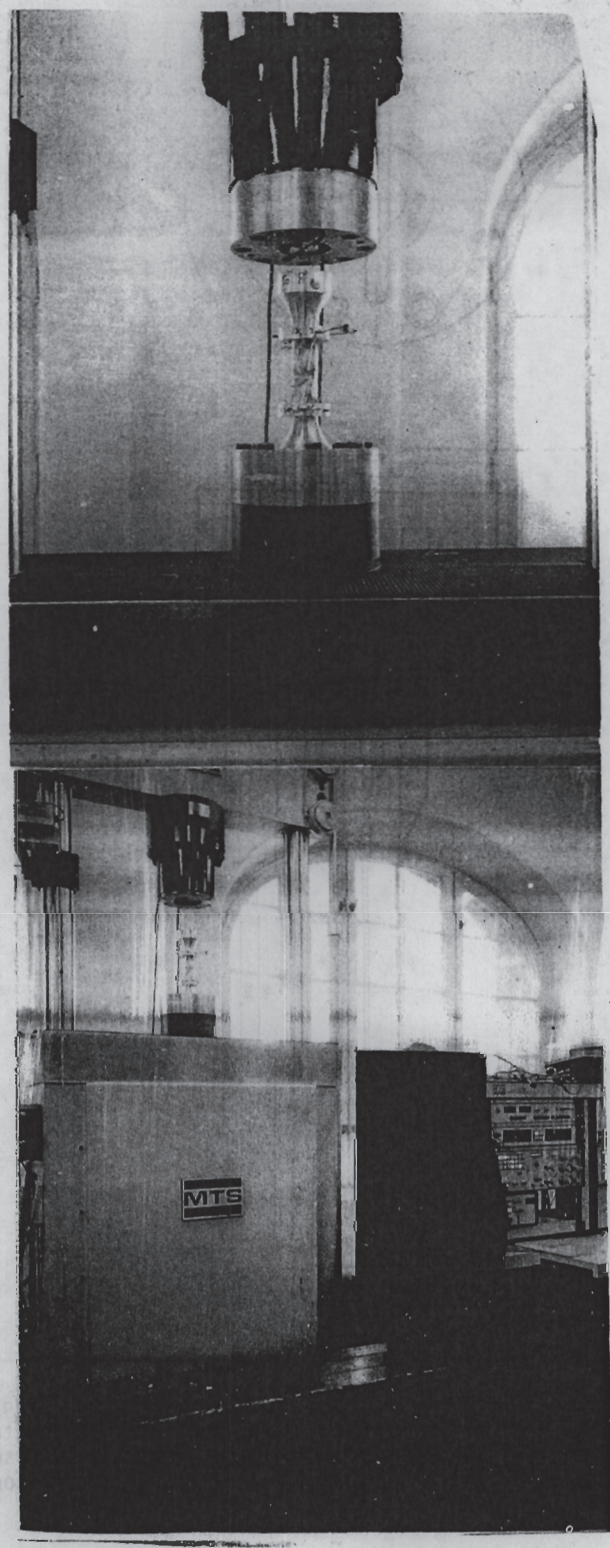

Fig 43 test specimen and fastenning ahachment

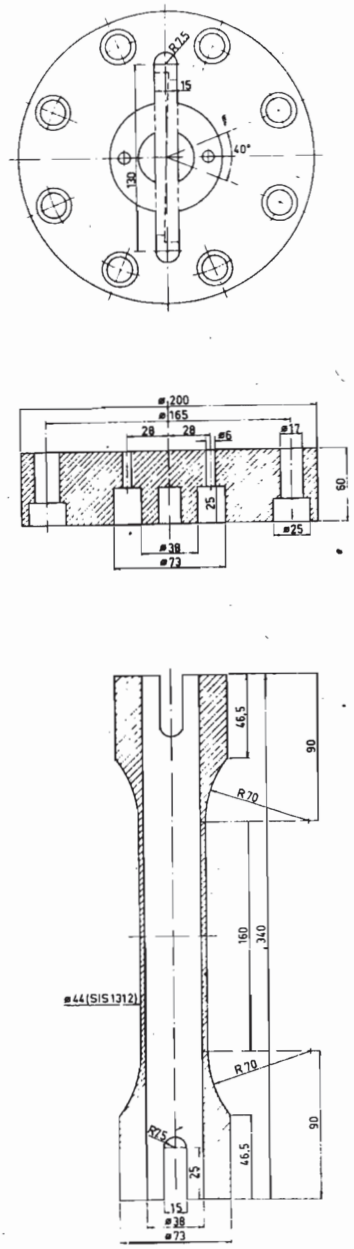

Fig ~~3.1.1~~ 4.4 Nominal dimensions of test specimens and fastening attachment. These were designed and manufactured at the Department of Building Statics and Structural Engineering by research engineers *Bertil Karlström* and *Kent Lindgren* in consultation with the author.